Plasticity state-dependent changes in visual cortex parvalbumin interneuron mRNA translation and chromatin

David Benacom, Camille Chataing, Jessica Apulei, Isabelle Queguiner, Alain Prochiantz, Ariel A Di Nardo*

Centre for Interdisciplinary Research in Biology (CIRB), Collège de France, CNRS, INSERM, Labex MemoLife, Université PSL, Paris, France.

*Correspondence: ariel.dinardo@college-de-france.fr

Abstract

The juvenile brain is shaped by critical periods of heightened plasticity whose timing is regulated by the maturation of parvalbumin interneurons. Gene expression during brain developmental is regulated by neuronal activity, which can trigger the formation of DNA double-strand breaks on early response genes regulatory elements. To determine if critical period plasticity induces double-strand breaks (γH2AX foci) and alters chromatin structure (DAPI foci) of parvalbumin cells, we analyzed the primary visual cortex of mice at peak ocular dominance plasticity (postnatal day P30) and in the non-plastic adult (at P90-P100). We also measured the expression of LINE-1 retrotransposons, known to induce double-strand breaks. Foci numbers and LINE-1 Orf1p expression were increased at P30 specifically in parvalbumin cells. TRAP-based RNA sequencing confirmed that LINE-1 translation in parvalbumin cells is activated at P30 compared to P100. ChABC injections in primary visual cortex were performed to determine whether reopened adult plasticity recapitulates the P30 translatome of parvalbumin cells. While the P30 TRAP was enriched for ion channel, postsynaptic membrane, and extracellular matrix components, the ChABC P100 TRAP was enriched for cytoskeletal structure and receptor binding proteins. Furthermore, ChABC treatment did not alter foci distribution or LINE-1 translation. These results suggest that juvenile critical periods promote genomic instability in parvalbumin cells and that adult plasticity reopened by ChABC is distinct from critical period plasticity.

Keywords

Critical period, perineuronal net, chondroitinase, double strand break, transposable elements

Introduction

During early postnatal brain development, sensory experience allows for the activity-dependent refinement of neuronal circuits. The seminal work of Hubel and Wiesel (1963) involving monocular deprivation and analysis of ocular dominance (OD) columns in primary visual cortex (V1) revealed heightened plasticity was restricted to a transient critical period (CP) in the juvenile animal. It has since been shown that CP timing is controlled by the maturation of cortical layer IV fast-spiking parvalbumin (PV) inhibitory interneurons affecting the inhibitory/excitatory (I/E) balance in layers III/IV (Hensch, 2005; Reh et al., 2020).

While changes in PV cell activity and connectivity are highly experience-dependent during the CP, the molecular changes that occur have not been thoroughly characterized at the gene expression and epigenetic levels. Histone deacetylation (HDAC) activity and DNA methylation are involved in the maturation and consolidation of V1 cortex, although specific cell types remain unknown (Baroncelli et al., 2016; Putignano et al., 2007; Tognini et al., 2015). Regarding PV cells, changes in their nuclear distribution of the methyl-DNA binding MeCP2 and their expression of *Gadd45b/g*, which can regulate DNA methylation, have been reported during V1 CP and induced adult plasticity (Apulei et al., 2019). Taken together, these findings suggest that epigenetic changes occur within PV cells during CP maturation.

The triggering of CP onset induces the expression of immediate-early genes (IEGs), a process demonstrated in neuronal cultures to involve the histone mark γH2Ax (Madabhushi et al., 2015). γH2Ax is a classic DNA double-stranded break (DSB) marker extensively studied in the context of irradiation, cancer, and oxidative stress, but appears to have an interesting physiological role in neurons, where it may be linked to cellular activity and the expression of long genes (Madabhushi et al., 2015; Shanbhag et al., 2019). DSBs can be produced by retrotransposons, in particular LINE-1, that encodes for ORF1p and ORF2p (Gasior et al., 2006). Interestingly, retrotransposon elements can be remodeled in V1 by HDAC inhibitors that induce adult plasticity (Lennartsson et al., 2015). We therefore set out to investigate PV cell changes in gene expression sand DSB formation during CPs and induced adult plasticity in V1.

Results

Parvalbumin cell epigenetic marks are altered during the critical period

Given that DSBs are important for the expression of IEGs (Madabhushi et al., 2015), we assessed whether DSBs are associated with postnatal juvenile CP plasticity and/or induced adult plasticity. We quantified the number of DSBs in PV cells in juvenile (peak CP at P30) and adult (P90) V1 by using the nuclear protein γH2AX, a marker for activity-dependent DSBs classically mediated by the type II topoisomerase (Fig. 1A). To more clearly quantify changes in γH2AX distribution, we developed a new tool based on a deep-learning strategy to identify PV cells and analyze the entire cellular and extracellular volume (*StarDist*, Schmidt et al., 2018) for staining of PV, perineuronal nets (PNNs), and nuclear foci after limited deep neuronal network training (see Material & Methods). PNNs are formed by the condensation of proteoglycans, hyaluronic acid and linking proteins and are key actors in the maturation of PV cells and consolidation of circuitry (Fawcett et al., 2019; Testa et al., 2019). We validated the classic changes observed during PV cell maturation in V1, such as a higher PV cell mean intensity (Fig. 1B) at P90 compared to P30 and a marked accumulation of PNNs stained by WFA at P90 (Fig. 1C). We also found a sharp decrease in γH2AX foci number at P90 compared to P30 (Fig. 1D) accompanied by a switch between a high number of low-intensity foci at P30, to a low number of high-intensity foci at P90 (Fig. 1E). These changes suggest global rearrangement of chromatin occurs between P30 and P90 in PV cells. Interestingly we also found that DAPI foci, a marker of heterochromatin, also change with age similarly to γH2AX foci in PV cells (Fig. 1D, E).

L1 translation is activated during the critical period

We investigated whether LINE-1 expression varies within PV cells during plasticity periods by using an antibody raised against ORF1p (a protein encoded by the LINE-1 bicistronic mRNA) (Blaudin de Thé et al., 2018). Quantification of expression before (P17), during (P30) and after the plasticity period (P100), reveals that ORF1p staining intensity is significantly higher at P30 within WFA+ cells (Fig. 2A). Our laboratory reported that EN1 homeoprotein transcription factor directly represses LINE-1 expression at the level of the ventral midbrain dopaminergic (mDA) neurons, thus limiting DSB formation in oxidative stress conditions or during ageing (Blaudin de Thé et al., 2018). Given that LINE-1 ORF2p, the second product of the bicistronic LINE-1 mRNA, has both endonuclease and reverse-transcriptase activities, we used stavudine (2',3'-didehydro-2',3'-

dideoxythymidine, d4T), a nucleoside analogue and strong LINE-1 reverse transcriptase inhibitor (Jones et al., 2008), to determine whether LINE-1 expression is implicated in DSB formation. Mice were infused in V1 for 3 days starting at P17 with either stavudine or vehicle and the changes in the average number of DSBs identified by γH2AX staining was analyzed at P20 (Fig. 2B, C). The number of DSBs was shown to be lower in WFA+ cells at P17 and to increase significantly at P20 (Fig. 2C, left panel) to levels similar to those of WFA- cells (Fig. 2C, right panel), which include neurons and glia cells. This increase was blocked by stavudine infusion, suggesting involvement of ORF2p activity in PV cells during CP onset (Fig. 2C, left panel). No changes were observed in WFA- cells (Fig. 2C, right panel).

Given that LINE-1 retro-transposition in non-mitotic cells remains controversial, and that ORF1p itself does not possess endonuclease activity, we sought to more precisely quantify LINE-1 expression during the CP. We crossed the *NuTrap-flox* mouse line, which allows for separate isolation of ribosomal-associated RNA in translation (TRAP) and nuclei (Roh et al., 2017), with the *PV::Cre* mouse line in order to express the NuTrap construct specifically in PV cells (Fig. 2D). This specificity was confirmed by staining for PV, WFA and GFP in V1 sections at P30, which showed that nearly 100% of PV-expressing cells also expressed GFP (Fig. 2E). Interestingly, while most GFP-expressing cells also expressed PV, some mice were found to have GFP in cells lacking PV, suggesting heterogeneous and subthreshold expression of PV in V1 at this age (Beurdeley et al., 2012; Lee et al., 2017). Using this *PV::Cre x NuTrap-flox* line (*PVNT*), we isolated and sequenced RNA from both nuclei and TRAP to determine differentially expressed genes (DEGs) and differentially translated genes (DTGs), respectively, at P30, the peak of V1 OD CP, and at P90, an adult non-plastic stage. We found a high expression of LINE-1 subfamilies in PV cell nuclei, although it was not significantly different between P30 and P90 at the nuclear level (Fig. 2F). In the TRAP fraction, we found lower levels of LINE-1 RNA (by approximately 100-fold, depending on the LINE-1 subfamily), but we confirmed a specific and significant upregulation of transcripts in translation at P30 compared to P90 in 10 LINE-1 subfamilies (Fig. 2G).

Parvalbumin cell translation is activated during the critical period

Based on the same dataset generated for the LINE-1 analysis, we compared overall DEG and DTG changes between P30 and P90. We sequenced the input fraction corresponding to bulk sequencing, the PV purified nuclei fraction and the PV purified ribosomal fraction at both ages.

First, we analyzed RNA from V1 tissue at P30 and P90 namely P30_input and P90_input, and identified 323 up-regulated genes and 186 down-regulated genes (Fig. 3A). We identified classic activity genes involved in CP such as *Egfr2*, *Arc*, *Fos* and *Nr4a1*, and found GO analysis of Cellular Component and Molecular Function to be highly enriched in synapse and junction formation (Fig. 3B), confirming the endogenous CP plasticity status of the tissue used for precipitation of PV nuclei and TRAP.

We found a large disparity between the PV-specific transcripts identified by nuclear and TRAP fractions. In our nuclear fraction, P30_nuc versus P90_nuc, we only report 40 DEGs between both time points, suggesting that transcription changes remain limited during and after the CP (Fig. 3C). In the TRAP fraction, we report more than 1000 DTGs, suggesting substantial translation regulation processes between both time points (Fig. 3D). GO Cellular components reveal an enrichment in post-synaptic, extracellular PNN, and perisynaptic components known to be implicated in PV cell maturation during the CP (Fig. 3E). GO Molecular Function analysis of DTGs shows strong enrichment in channel activity and transmembrane signaling components amongst other markers of neuronal activity (Fig. 3E). These results confirm that the changes observed in PV cell connectivity between P30 and P90 depend primarily on post-transcriptional regulation at the cell body and/or synaptic level.

Adult visual cortex plasticity with ChABC treatment involves alternate mechanisms compared to critical period plasticity

In order to determine whether an adult plasticity re-opening strategy also modifies the number or structure of γH2AX foci, we injected P90 mice unilaterally with ChABC, which is a well-established strategy for adult plasticity reopening that degrades proteoglycans and removes the PNNs of PV cells (Pizzorusso et al., 2002). We validated the efficiency of ChABC injection, as it resulted in a large reduction of the proportion of PV+WFA+ cells compared to PV+WFA- cells in the enzyme-injected hemisphere (Fig. 4A). ChABC treatment also decreased the number of observable PV+ cells (Fig. 4B). A similar decrease has been previously reported by our laboratory (Beurdeley et al., 2012) to be accompanied by restored PV cell numbers two weeks after ChABC treatment, whereby the decrease is not due to cell death but to PV staining transiently falling below detection levels. Here, we did not observe changes in PV intensity (Fig. 4C), as reported in the literature (Carceller et al., 2020). Thus, the discrepancy between the number of PV cells and PV

intensity might reflect a switch in PV intensity from mean basal expression to an undetectable level.

We also analyzed the effect of ChABC on various nuclear foci parameters, and found no change in either γH2AX foci number (Fig. 4D) or intensity (Fig. 4E). DAPI co-staining of chromocenters also shows no change in foci number or intensity (Fig. 4D, E). These results suggest that different mechanisms of plasticity are at play in the adult compared to those during physiological CP in the juvenile mouse.

In order to build upon our findings, we analyzed TRAP RNAseq to identify PV-specific ribosome-associated DTGs between ChABC treated and P90 control *PVNT* mice. We identify 696 upregulated genes and 126 downregulated genes (Fig. 4F). Strikingly, the GO Cellular Component analysis revealed that transcripts undergoing modulation in PV-specific TRAP were highly associated with cytoskeletal structure, in particular actin (Fig. 4G). Post-synaptic density components were also enriched that are known to be highly dependent on cytoskeleton structure for synaptic receptor anchorage and dendritic organization. The GO Molecular Function analysis revealed that upregulated proteins were enriched with actin binding and glutamate receptor binding function. (FDR $< 10^{-5}$). These results suggest that ChABC engages the translational regulation of core synaptic proteins and their associated cytoskeletal proteins that might take place in local synaptic compartments. Given the implication of the LINE-1 family translation in CP plasticity at P30, we also evaluated whether ChABC-induced adult plasticity similarly involves LINE-1 activation. We found no change in polysome-associated LINE-1 mRNA (Fig. 4H), suggesting that these LINE-1 subfamilies undergo specific translation only during the V1 CP.

Discussion

We demonstrated that some aspects of the chromatin status and genetic stability of PV cells, as suggested by γH2AX and DAPI foci, are modified during the physiological V1 OD CP. The increase in γH2AX foci number during the CP is antagonized by stavudine treatment, a potent inhibitor of LINE-1 retro-transposition activity. LINE-1 transcripts are highly represented in PV cell nuclei, and are found in the TRAP ribosomal fraction, suggesting that they are transcribed and translated in PV cells. During the CP peak, we observe a significant increase in LINE-1 transcripts in translation that is not recapitulated by inducing plasticity in the adult. This increase is reflected at the protein level with an increase in ORF1p staining at P30. Similarly, the comparison between

nuclear DEGs and polysome-associated DTGs at P30 and P90 reveals that a vast majority of the regulated transcripts are only observed in the polysome mRNA fraction. This suggests that regulation is generally not at the transcription level but, rather, at the initiation of translation. After ChABC treatment to reopen adult plasticity, γH2AX marks do not reverse to the increased levels observed during CP while DTGs relate to cytoskeletal changes and synaptic activity, suggesting that this treatment modifies morphological and physiological traits with little influence on chromatin structure. To confirm this hypothesis, a more direct analysis of the PV cell chromatin structure using methods such as Hi-C will need to be performed before, during and after CP and after induction of adult plasticity with ChABC.

Physiological significance of γH2AX staining and LINE-1 expression

We observed a transient increase in the number, but not intensity, of γH2AX foci in PV cells during V1 CP, followed by an almost twofold increase in mean γH2AX intensity at P90. This transient increase in foci numbers could be explained by the expression at P30 of IEGs, a class of genes which requires topo-isomerase related DSB formation for transcription (Madabhushi et al., 2015). The observation that stavudine, an inhibitor of the retro-transcriptase activity of ORF2p, prevents the increase of γH2AX foci number during CP is intriguing. Stavudine may cause allosteric changes in ORF2p conformation upon binding, thus impairing endonuclease activity or DNA binding. Accordingly, ORF2p endonuclease may act as a "topo-isomerase" during endogenous CP, but this assertion remains to be demonstrated, as the retro-transposase domain may also possess different functions, such as the generation of RNA-DNA hybrids (Schwertz et al., 2018). Another hypothesis is the increase in DSBs during the CP is a byproduct of a specific activity of ORF1p. ORF1p has an RNA binding activity and has been suggested to regulate RNA processing in p-bodies (Briggs et al., 2021). Specific functions of ORF1p might be required during CP, while associated unregulated ORF2p expression might result in unwanted endonuclease activity. In order to test this hypothesis and determine if ORF2p-dependent γH2AX foci formation is required for endogenous CP plasticity, we could infuse stavudine over the course of the CP coupled with MD. An absence of OD shift would then demonstrate the role of ORF2p for CP plasticity through the formation of breaks revealed by γH2AX foci. It would also be of great interest to evaluate the distribution of H3K27me3 marks, which have been shown to be remodeled by LINEs for the fine-tuning of gene expression during brain development (Mangoni et al., 2023).

Re-opening strategies do not recapitulate endogenous CP mechanisms

The development of tools to assess chromatin foci and genetic instability in PV cells has enabled us to determine important new parameters for plasticity. The nature of chromatin changes differs between physiological CP and plasticity reopening, as shown by the comparison of γH2AX staining between P30, P90 and in ChABC-injected adult mice. Interestingly, while we first analyzed DAPI as a control, we reported a significant decrease in chromocenter number between P30 and P90, once again not recapitulated with ChABC treatment. However, we cannot totally preclude that there exist several independent pathways to reopen plasticity in the adult and that they differ according to the strategy. Strategies include ChABC, employed in this study, as well as fluoxetine, HDAC inhibitors, and single chain antibodies against OTX2 (Bernard et al., 2016; Casarotto et al., 2021; Silingardi et al., 2010).

Taken together, these observations lead us to propose that juvenile CP plasticity and induced adult plasticity are distinct phenomena. Analyses of the molecular actors identified by TRAP either for physiological CP or re-opened plasticity reveal the high diversity of mechanisms underlying plasticity, and provide an extensive resource on pathways which require validation in future studies. Some re-opening strategies might provide useful adaptive pathways for an altered functional network, but could come at the expense of other physiological functions, suggesting that further characterization of the safety of these methods is needed. Further studies comparing the transcriptomic signature of PV cells subjected to a plasticity reopening strategy with or without physical challenge could reveal different genes involved in a plasticity "permissive" state, and genes actually responsible for plastic changes, or "effectors" genes. Identification of plasticity permissive genes in comparison to plasticity effector genes in future studies might provide an important framework to consider when assessing plasticity re-opening strategies.

Material and methods

Mice and surgery

The C57Bl/6 J mice were purchased from Janvier Laboratories, while *PV::Cre* mice and *NuTrap* mice were obtained from Jackson Labs, USA. The *PVNT* mice were generated by crossing *PV-Cre* females and *NuTrap* males to avoid spurious recombination in the testis, which have been shown to transiently express PV. Stereotaxic infusions into V1(lambda: x = 1.7 mm, y = 0 mm, z = 0.5

mm) with 3-day osmotic mini pump (Alzet 1003D, Charles River Laboratories) were used to deliver stavudine (d4T, 10 µM, Sigma Y0000408) diluted in 0.9% NaCl. Recombinant ChABC (Bio-Techne) was injected in V1 (lambda: x = ±1.7 mm, y = 0 mm, z = 0.5 mm) with a single dose of 0.5 µl (50 U/mL) at a rate of 0.1 µl/min using a Hamilton 1701 syringe mounted with a 33G needle. All animal procedures, including housing, were carried out in accordance with the recommendations of the European Economic Community (2010/63/UE) and the French National Committee (2013/118). For surgical procedures, animals were anesthetized with xylazine (Rompun 2%, 5 mg/kg) and ketamine (Imalgene 500, 80 mg/kg). For biochemical analysis, mice either underwent transcardial perfusion or were sacrificed by cervical elongation.

Immunohistochemistry

Mice were perfused transcardially with PBS followed by 4% paraformaldehyde prepared in PBS. Brains were postfixed for 24 h at 4 °C and immunohistochemistry was performed on cryosections (20 µm) encompassing the entire visual cortex. Heat-induced antigen retrieval in 10 mM sodium citrate was performed prior to overnight primary antibody incubation at 4 °C. Primary antibodies included anti PV (rabbit, Swant 27) anti-γH2AX (mouse, 1/200, millipore clone JBW301), anti-ORF1p (guinea pig, 1/ 200, in house), and biotinylated WFA (1/100, Sigma L1516). Secondary antibodies were Alexa Fluor-conjugated (Molecular Probes). Images were acquired with a Leica SP5 or LSM 800(Zeiss) confocal microscope with 20 µm of the slide acquired with a 1 µm step.

Image Analysis

Microscopy analysis was conducted using using ImageJ. For manual foci quantification, a Z projection was applied before manual foci counting. For intensity quantification, a mask was traced following inner WFA staining, and measured in the Orf1p channel. An in-house script used a custom analysis macro in Java for image analysis, using a trained model for automatic PV and PNN detection. Briefly, we trained the model to detect PNN and PV staining based on a subsampling of random images in the datasets. DAPI signal within PV masks was used for nuclear delimitation. Foci detection was performed using an in-house script with user-defined parameters, and validated on a subset of 10 images.

TRAP protocol

Brain V1 cortices of *PVNT* mice were manually dissected with a particular emphasis on myelin removal, and placed into a pre-chilled 2 ml dounce containing 1 ml cold lysis buffer (50mM TrisHCl 7,5 + 100mM KCl + 12mM $MgCl_2$ + 1% NP40 + 1mM DTT + 100 µg/ml cycloheximide (sigma) + 0,4 U/µl RNAse OUT + Protease inhibitor (Pierce) 1X). Dounce with a loose pestle was performed 10 times, followed by a tight pestle for 10 strokes, 5' incubation, and 10 supplementary strokes. Homogenates were filtered on 40 µm strainer and transferred to a pre-chilled 2 ml LoBind tube. Homogenates were subsequently centrifuged at 4 °C, 10,000 rcf for 10 min. A 50 µl sample of supernatant was kept as input, and the remaining supernatant was transferred to a pre-chilled 1.5 ml LoBind tube. A 10' pre-clear step was performed, using 10µl un-conjugated DynaBeads Protein G (Thermofisher, 1003D) per sample at 4°. Beads were removed with a Dynamag magnet (Thermofisher) and samples were incubated with 1 µg anti-GFP antibody (ab290, abcam) for 1h at 4°. DynaBeads Protein G (Thermofisher, 1003D) were blocked in 1 mL lysis buffer supplemented with 2% BSA and 0.2 mg/ml yeast tRNA for 3x 1' incubation, and resuspended in their original volume. 30µL Dynabeads Protein G were added in each sample, for a supplementary 2h incubation at 4 °C. Samples were placed on a DynaMag magnet for 1 min until complete clearing of the beads in solution. Beads were washed 3 times with high salt lysis buffer (50mM TrisHCl 7,5 + 300mM KCl + 12mM $MgCl_2$ + 1% NP40 + 2mM DTT + 100 µg/ml cycloheximide + 0,4 U/µl RNAse OUT + IP 1X). After the third wash, samples were removed from the magnet and beads were resuspended in 500 µL QIAzol and kept at -80° until RNA extraction using QIAgen Micro Kit with standard procedure. Double DNAse treatment was performed. Purified RNA were quantified on a Qubit 4 device and analyzed on a BioAnalyzer for quality control.

Nuclear isolation protocol

Brain V1 cortices of *PVNT* mice were manually dissected and placed into a pre-chilled 2 ml dounce containing 1 ml cold homogenization buffer (HB) 1X (sucrose 0.25M, inhibitor protease 1X, DTT 1mM, spermidine 0.5 mM, spermine 0.15 mM, NP40 0.3%, H2O). HB was supplemented with 10 µl RiboLock per ml of HB. Dounce with a loose pestle was performed 10 times, followed by a tight pestle for 10 strokes, 5' incubation, and 10 supplementary strokes. Homogenates were filtered on 40 µm strainer and transferred to a pre-chilled 2 ml LoBind tube. Homgenate were subsequently centrifugated at 4 °C, 350 rcf, soft settings for 5 min in swinging

buckets. 50 µl of supernatant was removed as input (containing cytoplasmic RNAs) and transferred to a pre-chilled 1.5 ml LoBind tube. Nuclei were gently resuspended in a total volume of 400 µl 1x HB and mixed with 50% optiprep solution to a final 25% optiprep. 600 µl of 30% optiprep solution was laid under the 25% mixture. The gradient was centrifugated in a pre-chilled swinging bucket centrifuge, for 10 min at 4 °C, 3000 rcf with soft settings. The top layer was slowly removed down to within 50 µl of the nuclei pellet. The nuclei pellet was then resuspended in FACS Buffer (BSA 0.1%, RNAse-IN 0.01%, 0.1% triton, PBS) to a volume of 500 µL. FACS gating were performed using nuclei extracted from WT mice using the same procedure. The GFP population was sorted directly into QIAzol and kept at -80 °C until RNA extraction using QIAgen Micro Kit with standard procedure. Double DNAse treatment was performed. Purified RNA were quantified on a Qubit 4 device and analyzed on a BioAnalyzer for quality control.

Sequencing & Bioinformatic analysis

Samples were sequenced by the Curie Institute Genomics facility with the SMARTer Stranded Total RNA-Seq Kit Pico Input Mammalian. Bioinformatic analysis was conducted using *OneStopRNAseq* (Li et al., 2020) with standard parameters for DEG analysis, and *SalmonTE* for transponable element analysis (Jeong et al., 2018). *Enrichr* was used for GO analysis (Xie et al., 2021).

Statistical Analysis

Statistical analysis was performed on Prism 9 (GraphPad). Pairwise comparison was performed with Student t-test, while multiple group analyses were done with ANOVA (one- or two-way) followed by Bonferroni correction. Changes in frequency distribution were assessed by Kolmogorov–Smirnov test.

Acknowledgements

We would like to thank Damien Testa and Uma Mani for technical assistance. Funding was provided by the European Research Council Advanced Grant (ERC-2013-ADG-339379) and by the NeuroGlia Foundation for supporting research costs and salaries.

References

Apulei J, Kim N, Testa D, Ribot J, Morizet D, Bernard C, Jourdren L, Blugeon C, Di Nardo AA, Prochiantz A. 2019. Non-cell Autonomous OTX2 Homeoprotein Regulates Visual Cortex Plasticity Through Gadd45b/g. *Cereb Cortex* **29**:2384–2395. doi:10.1093/cercor/bhy108

Baroncelli L, Scali M, Sansevero G, Olimpico F, Manno I, Costa M, Sale A. 2016. Experience Affects Critical Period Plasticity in the Visual Cortex through an Epigenetic Regulation of Histone Post-Translational Modifications. *J Neurosci* **36**:3430–3440. doi:10.1523/JNEUROSCI.1787-15.2016

Bernard C, Vincent C, Testa D, Bertini E, Ribot J, Di Nardo AA, Volovitch M, Prochiantz A. 2016. A Mouse Model for Conditional Secretion of Specific Single-Chain Antibodies Provides Genetic Evidence for Regulation of Cortical Plasticity by a Non-cell Autonomous Homeoprotein Transcription Factor. *PLOS Genet* **12**:e1006035. doi:10.1371/journal.pgen.1006035

Beurdeley M, Spatazza J, Lee HHC, Sugiyama S, Bernard C, Di Nardo AA, Hensch TK, Prochiantz A. 2012. Otx2 binding to perineuronal nets persistently regulates plasticity in the mature visual cortex. *J Neurosci* **32**:9429–9437. doi:10.1523/JNEUROSCI.0394-12.2012

Blaudin de Thé F, Rekaik H, Peze-Heidsieck E, Massiani-Beaudoin O, Joshi RL, Fuchs J, Prochiantz A. 2018. Engrailed homeoprotein blocks degeneration in adult dopaminergic neurons through LINE-1 repression. *EMBO J* **37**:e97374. doi:10.15252/embj.201797374

Briggs EM, McKerrow W, Mita P, Boeke JD, Logan SK, Fenyö D. 2021. RIP-seq reveals LINE-1 ORF1p association with p-body enriched mRNAs. *Mob DNA* **12**:5. doi:10.1186/s13100-021-00233-3

Carceller H, Guirado R, Ripolles-Campos E, Teruel-Marti V, Nacher J. 2020. Perineuronal Nets Regulate the Inhibitory Perisomatic Input onto Parvalbumin Interneurons and γ Activity in the Prefrontal Cortex. *J Neurosci* **40**:5008–5018. doi:10.1523/JNEUROSCI.0291-20.2020

Casarotto PC, Girych M, Fred SM, Kovaleva V, Moliner R, Enkavi G, Biojone C, Cannarozzo C, Sahu MP, Kaurinkoski K, Brunello CA, Steinzeig A, Winkel F, Patil S, Vestring S, Serchov T, Diniz CRAF, Laukkanen L, Cardon I, Antila H, Rog T, Piepponen TP, Bramham CR, Normann C, Lauri SE, Saarma M, Vattulainen I, Castrén E. 2021. Antidepressant drugs act by directly binding to TRKB neurotrophin receptors. *Cell* **184**:1299-1313.e19. doi:10.1016/j.cell.2021.01.034

Fawcett JW, Oohashi T, Pizzorusso T. 2019. The roles of perineuronal nets and the perinodal extracellular matrix in neuronal function. *Nat Rev Neurosci* **20**:451–465. doi:10.1038/s41583-019-0196-3

Gasior SL, Wakeman TP, Xu B, Deininger PL. 2006. The Human LINE-1 Retrotransposon Creates DNA Double-strand Breaks. *J Mol Biol* **357**:1383–1393. doi:10.1016/j.jmb.2006.01.089

Hensch TK. 2005. Critical period plasticity in local cortical circuits. *Nat Rev Neurosci* **6**:877–888. doi:10.1038/nrn1787

Hubel DH, Wiesel TN. 1963. Shape and arrangement of columns in cat's striate cortex. *J Physiol* **165**:559–568. doi:10.1113/jphysiol.1963.sp007079

Jeong H-H, Yalamanchili HK, Guo C, Shulman JM, Liu Z. 2018. An ultra-fast and scalable quantification pipeline for transposable elements from next generation sequencing dataBiocomputing 2018. WORLD SCIENTIFIC. pp. 168–179. doi:10.1142/9789813235533_0016

Jones RB, Garrison KE, Wong JC, Duan EH, Nixon DF, Ostrowski MA. 2008. Nucleoside Analogue Reverse Transcriptase Inhibitors Differentially Inhibit Human LINE-1 Retrotransposition. *PLoS One* **3**:e1547. doi:10.1371/journal.pone.0001547

Lee HHC, Bernard C, Ye Z, Acampora D, Simeone A, Prochiantz A, Di Nardo AA, Hensch TK. 2017. Genetic Otx2 mis-localization delays critical period plasticity across brain regions. *Mol Psychiatry* **22**:680–688. doi:10.1038/mp.2017.1

Lennartsson A, Arner E, Fagiolini M, Saxena A, Andersson R, Takahashi H, Noro Y, Sng J, Sandelin A, Hensch TK, Carninci P. 2015. Remodeling of retrotransposon elements during epigenetic induction of adult visual cortical plasticity by HDAC inhibitors. *Epigenetics Chromatin* **8**:55. doi:10.1186/s13072-015-0043-3

Li R, Hu K, Liu H, Green MR, Zhu LJ. 2020. OneStopRNAseq: A Web Application for Comprehensive and Efficient Analyses of RNA-Seq Data. *Genes (Basel)* **11**:1165. doi:10.3390/genes11101165

Madabhushi R, Gao F, Pfenning AR, Pan L, Yamakawa S, Seo J, Rueda R, Phan TX, Yamakawa H, Pao P-C, Stott RT, Gjoneska E, Nott A, Cho S, Kellis M, Tsai L-H. 2015. Activity-Induced DNA Breaks Govern the Expression of Neuronal Early-Response Genes. *Cell* **161**:1592–1605. doi:10.1016/j.cell.2015.05.032

Mangoni D, Simi A, Lau P, Armaos A, Ansaloni F, Codino A, Damiani D, Floreani L, Di Carlo

V, Vozzi D, Persichetti F, Santoro C, Pandolfini L, Tartaglia GG, Sanges R, Gustincich S. 2023. LINE-1 regulates cortical development by acting as long non-coding RNAs. *Nat Commun* **14**:4974. doi:10.1038/s41467-023-40743-7

Pizzorusso T, Medini P, Berardi N, Chierzi S, Fawcett JW, Maffei L. 2002. Reactivation of Ocular Dominance Plasticity in the Adult Visual Cortex. *Science (80-)* **298**:1248–1251. doi:10.1126/science.1072699

Putignano E, Lonetti G, Cancedda L, Ratto G, Costa M, Maffei L, Pizzorusso T. 2007. Developmental Downregulation of Histone Posttranslational Modifications Regulates Visual Cortical Plasticity. *Neuron* **54**:177. doi:10.1016/j.neuron.2007.03.011

Reh RK, Dias BG, Nelson CA, Kaufer D, Werker JF, Kolb B, Levine JD, Hensch TK. 2020. Critical period regulation across multiple timescales. *Proc Natl Acad Sci* **117**:23242–23251. doi:10.1073/pnas.1820836117

Roh HC, Tsai LT-Y, Lyubetskaya A, Tenen D, Kumari M, Rosen ED. 2017. Simultaneous Transcriptional and Epigenomic Profiling from Specific Cell Types within Heterogeneous Tissues In Vivo. *Cell Rep* **18**:1048–1061. doi:10.1016/j.celrep.2016.12.087

Schmidt U, Weigert M, Broaddus C, Myers G. 2018. Cell Detection with Star-Convex Polygons. *Lect Notes Comput Sci* 265–273. doi:10.1007/978-3-030-00934-2_30

Schwertz H, Rowley JW, Schumann GG, Thorack U, Campbell RA, Manne BK, Zimmerman GA, Weyrich AS, Rondina MT. 2018. Endogenous LINE-1 (Long Interspersed Nuclear Element-1) Reverse Transcriptase Activity in Platelets Controls Translational Events Through RNA–DNA Hybrids. *Arterioscler Thromb Vasc Biol* **38**:801–815. doi:10.1161/ATVBAHA.117.310552

Shanbhag NM, Evans MD, Mao W, Nana AL, Seeley WW, Adame A, Rissman RA, Masliah E, Mucke L. 2019. Early neuronal accumulation of DNA double strand breaks in Alzheimer's disease. *Acta Neuropathol Commun* **7**:77. doi:10.1186/s40478-019-0723-5

Silingardi D, Scali M, Belluomini G, Pizzorusso T. 2010. Epigenetic treatments of adult rats promote recovery from visual acuity deficits induced by long-term monocular deprivation. *Eur J Neurosci* **31**:2185–2192. doi:10.1111/j.1460-9568.2010.07261.x

Testa D, Prochiantz A, Di Nardo AA. 2019. Perineuronal nets in brain physiology and disease. *Semin Cell Dev Biol* **89**:125–135. doi:10.1016/j.semcdb.2018.09.011

Tognini P, Napoli D, Tola J, Silingardi D, Della Ragione F, D'esposito M, Pizzorusso T. 2015.

Experience-dependent DNA methylation regulates plasticity in the developing visual cortex. *Nat Neurosci* **18**:956–958. doi:10.1038/nn.4026

Xie Z, Bailey A, Kuleshov M V, Clarke DJB, Evangelista JE, Jenkins SL, Lachmann A, Wojciechowicz ML, Kropiwnicki E, Jagodnik KM, Jeon M, Ma'ayan A. 2021. Gene Set Knowledge Discovery with Enrichr. *Curr Protoc* **1**:e90. doi:10.1002/cpz1.90

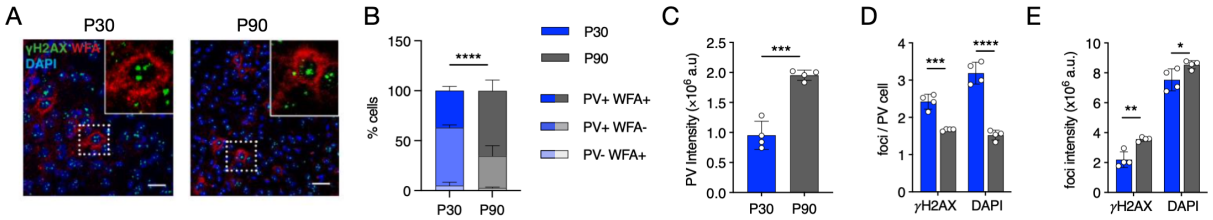

Figure 1. Parvalbumin cell epigenetic marks are altered during the critical period.

A. Representative immunostainings for γH2AX and WFA in V1 layer IV of WT mice at P30 and P90. Scale bar, 40 µm.

B-C. Quantification of cells double-stained or not for PV and WFA (B) and of PV staining intensity (C).

D-E. Quantification of foci number (E) and staining intensity (F) for γH2AX and DAPI in PV cells.

Values mean ± SEM; unpaired t-test in C-E; ANOVA in B; $n = 4$ mice; *$p < 0.05$, **$p < 0.01$, ***$p < 0.001$, ****$p < 0.0001$.

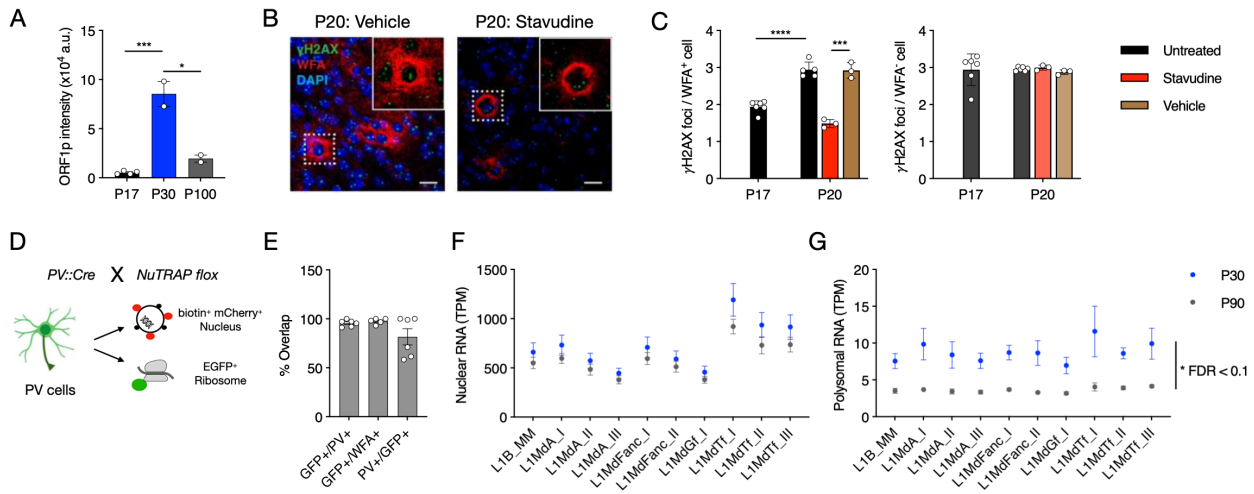

Figure 2. L1 translation is activated during the critical period.

A. Quantification of ORF1p staining intensity in WFA+ cells of V1 in WT mice.

B. Staining of γH2AX and WFA in V1 layer IV of mice infused with either stavudine or vehicle from P17 to P20. Scale bar, 40 µm.

C. Quantification of γH2AX foci in WFA^+ cells (left panel) and WFA^- cells (right panel) in WT mice and in mice treated with Stavudine or Vehicle.

D. Schematic of the breeding strategy to obtain the RNA of either nuclei or polysomes specifically from cortical PV cells.

E. Quantification of staining for PV, WFA, and GFP in V1 layer IV to evaluate expression co-localization at P30 (% overlap).

F. The expression of L1 subfamilies in purified PV cell nuclei from V1 of P30 and P90 WT mice measured by transcript per million (TPM).

G. The expression in TPM of L1 subfamilies in PV cell TRAP from V1 of P30 and P90 WT mice. Values in A, C, and E, mean ± SEM; unpaired t-test; n = 2-5 mice; *$p < 0.05$, ***$p < 0.001$, ****$p < 0.0001$. Values in F and G, mean ± SD; N = 3-4 samples; *FDR< 0.01 for each subfamily in G.

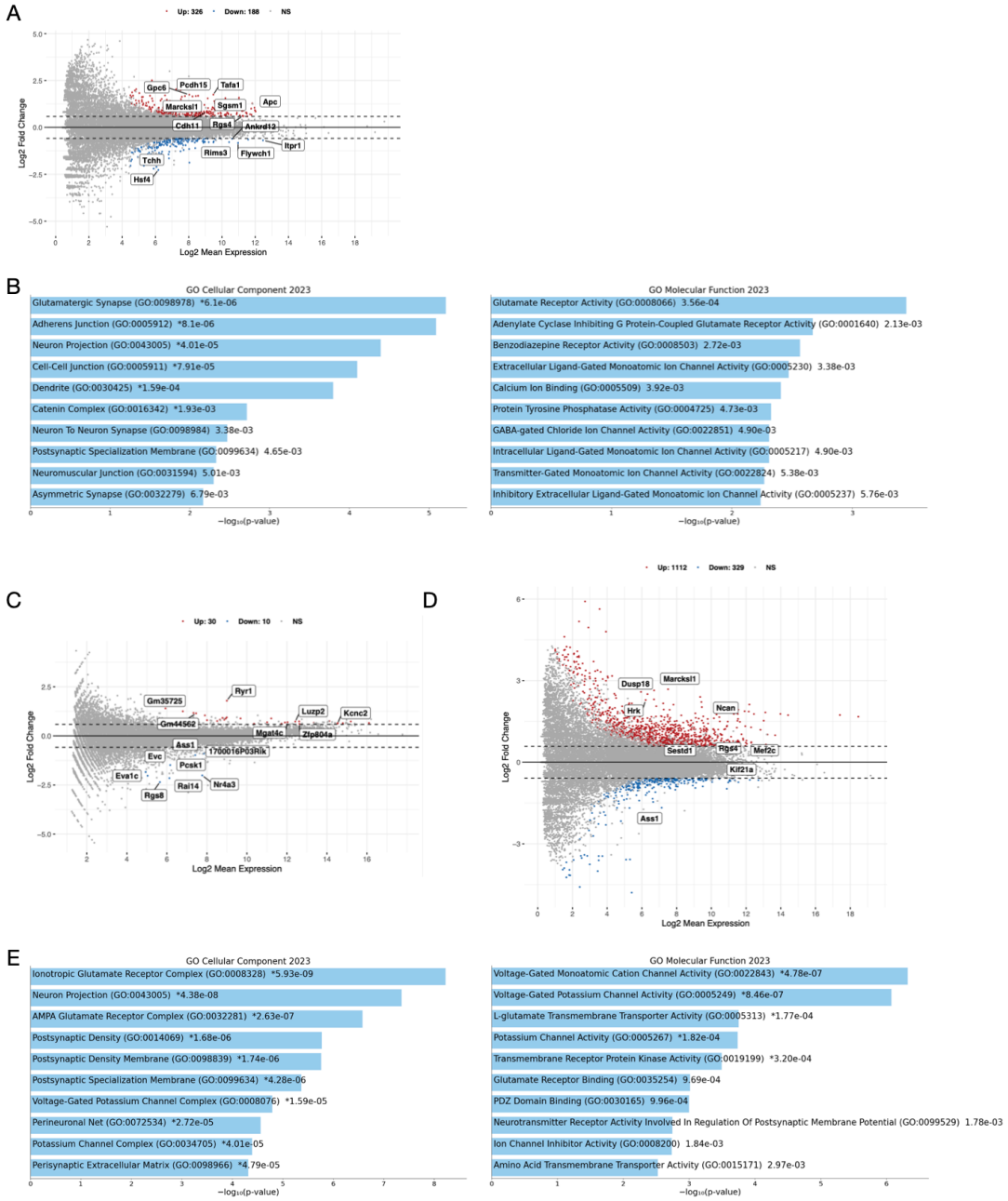

Figure 3. Parvalbumin cell translation is activated during the critical period

A. MA plot with Log_2(fold change) as a function of Log_2(mean expression) showing differential expression between P30 and P90 obtained from RNAseq of the input fractions.

B. Input fraction RNAseq GO analysis (Enrichr software) of Cellular Component, for genes involved in the composition of a specific cellular compartment, and of Molecular Function, for protein functional classes.

C-D. MA plots showing differential expression between P30 and P90 obtained from RNAseq of PV cell nuclear fractions (C) and PV cell TRAP fractions (D).

E. TRAP RNAseq GO analysis of Cellular Component and Molecular Function.

Red dots and blue dots indicate significantly (FDR < 0.1) upregulated and downregulated genes, respectively (N = 3-4 samples). *FDR enrichment value.

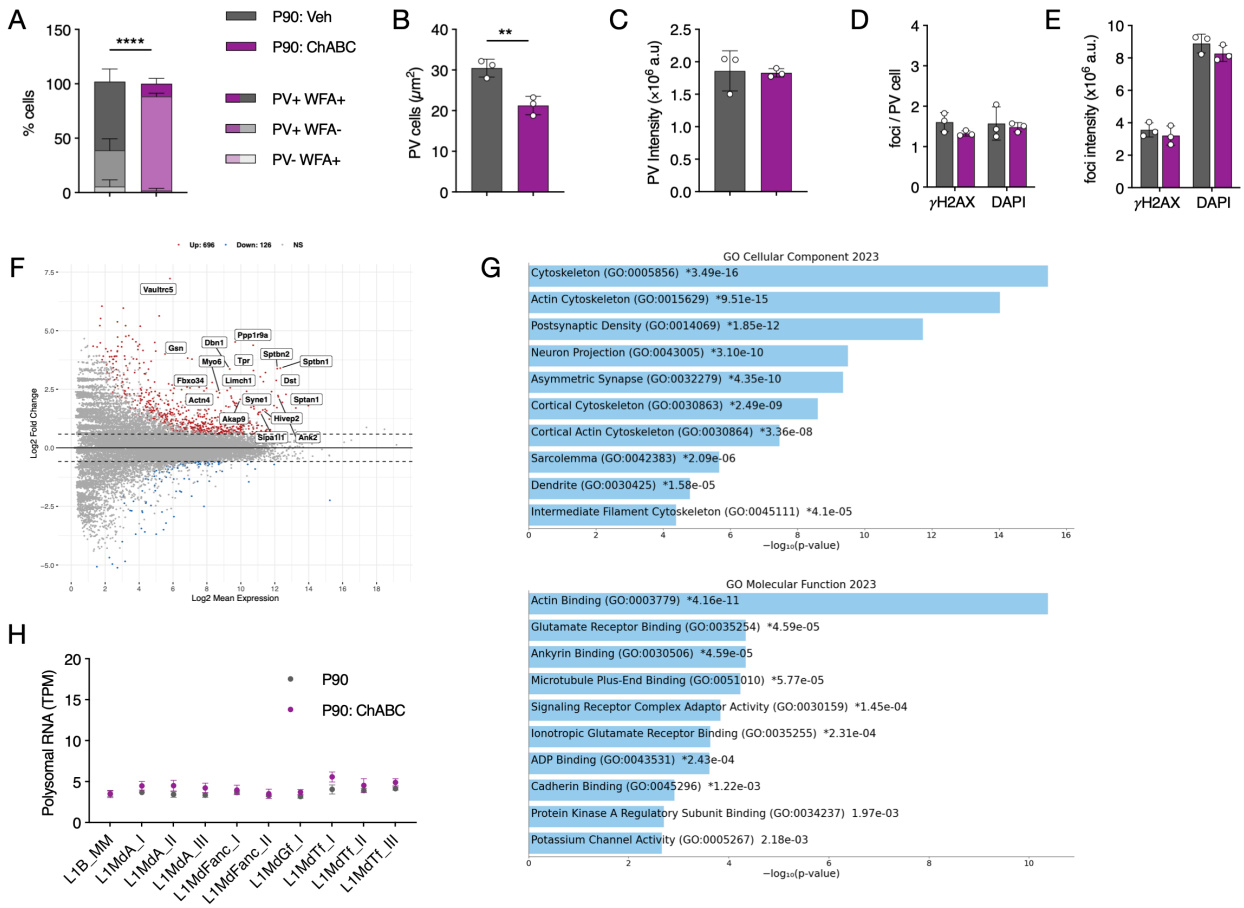

Figure 4. Adult visual cortex plasticity with ChABC treatment involves alternate mechanisms compared to critical period plasticity

A-C. Quantification of cells double-stained or not for PV and WFA (A), PV cell numbers (B), and PV staining intensity (C).

D-E. Quantification of foci number (D) and staining intensity (E) for γH2AX and DAPI in PV cells.

F. MA plots with Log_2(fold change) as a function of Log_2(mean expression) showing differentially translated genes between vehicle and ChABC treated mice obtained from RNAseq of PV cell TRAP fractions. Red dots and blue dots indicate significantly (FDR < 0.1) upregulated and downregulated genes, respectively ($N = 3$ samples).

G. TRAP RNAseq GO analysis (Enrichr software) of Cellular Component, for genes involved in the composition of a specific cellular compartment, and of Molecular Function, for protein functional classes. *FDR enrichment value.

H. The expression in TPM of L1 subfamilies in PV cell TRAP from V1 of P90 WT and ChABC-injected mice.

Values in A-E, mean ± SEM; unpaired t-test; $n = 3$ mice; $^{**}p < 0.01$, $^{****}p < 0.0001$.